Q-switched pulsing lasers subject to delayed feedback: A model comparison

Soizic Terrien,* Bernd Krauskopf, and Neil G. R. Broderick
The Dodd-Walls Centre for Photonic and Quantum Technologies, The University of Auckland, 38 Princes Street, Auckland 1010, New Zealand

Lina Jaurigue and Kathy Lüdge
Institut fur Theoretische Physik, Technische Universitat Berlin, 10623 Berlin, Germany

(Received 25 May 2018; published 9 October 2018)

We report theoretical and numerical results on the dynamics of pulsing lasers with gain and absorber sections subject to delayed optical self-feedback. We consider two modeling approaches, with the Yamada model, on the one hand, and a delay model for ring-cavity mode-locked lasers, on the other hand. We focus on the limit where a single mode is involved, and we show that, in the case without feedback, the dynamics of both models show very good quantitative agreement: *Q*-switched periodic pulsing regimes with similar properties are observed. A bifurcation analysis unveils the conditions for the dynamics to be similar in both systems when an additional delayed feedback term is considered: in particular, what is important is to match the period and the width of the pulsing dynamics of the solitary lasers. Our results show that the simple Yamada model can catch the essence of the dynamics of pulsing lasers with feedback in the limit of single-mode systems. This may considerably simplify, in future work, the investigation of the dynamics of certain self-pulsing lasers with feedback.

DOI: 10.1103/PhysRevA.98.043819

I. INTRODUCTION

Sources of short, high-amplitude pulses of light are widely used in many applications, such as telecommunications and optical signal processing [1]. As such, they have attracted considerable attention in the last decades, and self-pulsing regimes have been observed in a variety of laser systems. This includes fiber laser cavities [2], vertical cavity surface-emitting lasers [3], and semiconductor lasers with integrated saturable absorbers [4,5].

Despite similar features of the pulsing dynamics, the underlying physical mechanism for self-pulsations can be fundamentally different from one device to another. *Q*-switching is arguably the simplest mechanism for self-pulsating lasers, as it relies only on variable losses in the laser cavity [6]. In the case of passive *Q*-switching, these are induced by a saturable absorber medium, in which the transmission increases dramatically when the light intensity in the cavity exceeds a given threshold. Because the intracavity intensity is initially low, the losses due to the saturable absorber are high and most of the energy provided by pumping the gain medium is stored in the gain section. When the gain overcomes the losses, the intensity starts to increase, which eventually saturates the absorber and causes a sudden drop of the cavity losses. The light intensity hence increases rapidly until all the energy stored in the device has been released, at which point the intensity drops back to a very low value. As the process repeats, short, high-amplitude pulses of light are emitted, in between which the intensity is practically 0 while the gain recovers. This mechanism for self-pulsations does not involve the interaction between different modes of the laser cavity, and microlasers with integrated saturable absorbers, which are essentially single mode due to their small size, have been designed specifically to feature a *Q*-switching instability [4,7]. Such systems are described accurately by the Yamada rate equations, a system of three ordinary differential equations (ODEs) for the gain, the absorption, and the light intensity [8,9], which is described in more detail in the next section. In particular, it has been shown that the phase of the electric field is not relevant for the description of these systems [10].

Self-pulsations in lasers can also be achieved by mode-locking. This technique relies on the phase synchronization of a large number of longitudinal modes of the laser cavity to produce trains of very short optical pulses at a high repetition rate [11–13]. Compared to *Q*-switched lasers, mode-locked lasers require a different design to allow a large number of modes to contribute to the laser emission and to induce a fixed phase relationship between them. The number of modes involved in the lasing process is given by the spectral width of the amplifying medium and can be reduced by spectral filter elements. Mathematical models for mode-locked lasers are more complex than models for *Q*-switched lasers; in particular, they have to take into account the phase of the complex electric field. Many theoretical studies have adopted a traveling-wave equations approach [14,15]. This results in accurate modeling of the dynamics, which requires time-consuming numerical simulations and complicates a systematic bifurcation analysis. Alternatively, a delay model relying on the assumption of unidirectional light propagation in the laser cavity has been proposed in [16] and [17] in the form of delay differential equations (DDEs). Although DDEs are mathematically more complex than ODEs, bifurcation analysis can be performed with advanced numerical methods [18–20], yielding global knowledge of the dependence of the dynamics on the parameters.

*s.terrien@auckland.ac.nz

Besides several mode-locked regimes, mode-locked lasers can also exhibit a Q-switching instability, which can lead to a pulsing regime with a modulated amplitude, referred to as Q-switched mode-locking [21]. In this case, if the spectral filter width is reduced such that only a single-cavity mode can contribute to the lasing process, mode-locking can no longer occur, but the Q-switching instability remains [13]. In this particular case, the Yamada model and the DDE model for mode-locked lasers (DDE MLL) describe the same physical phenomenon, but with very different equations.

Pulsing lasers, whether mode-locked or Q-switched, are highly sensitive to perturbations: small amounts of noise can trigger substantial fluctuations of the repetition rate of pulses [22–24]. This timing-jitter phenomenon is detrimental to most applications. Delayed optical self-feedback has been proposed as an efficient technique to reduce timing-jitter significantly and, more generally, to allow better control of the pulsing dynamics [12,24]. The effect of feedback has been studied numerically in both the Yamada model and the DDE MLL model, where the feedback is introduced, respectively, via an external mirror and through an additional integrated ring cavity. It is noteworthy that in the presence of feedback, both models are systems of DDEs, with one delay time for the Yamada model and two different delay times for the DDE MLL model. Extensive bifurcations analysis has been performed [21,24–26], which focused on the feedback-induced dynamics in a Q-switched laser in the excitable regime and in a laser in the fundamental mode-locked regime.

We consider here the effect of feedback when both solitary lasers are in the Q-switched pulsing regime. We first present the Yamada model and the DDE MLL model in more detail and show how they relate to each other. We then perform a bifurcation analysis of both models without feedback and compare their dynamics, with a focus on the dependence of the pulse width and pulsing period of the Q-switched regime on the pump and absorption levels. With the numerical continuation toolbox DDE-Bitool for delay systems [18–20], we then perform a bifurcation analysis of both models with feedback and unveil the conditions under which the feedback-induced dynamics will be qualitatively the same. In particular, we investigate how small changes in the width and period of the pulsing solution of the solitary laser (i.e., without feedback) affect the feedback-induced dynamics. As such, we demonstrate that, over a large range of parameters, the dynamics of the DDE MLL model in the limit of a single active mode can be accurately described by the simpler Yamada model.

II. MODEL EQUATIONS

The Yamada model [8] describes the dynamics of Q-switched single-mode semiconductor lasers. It is originally a system of three ODEs for the gain G, the absorption Q, and the intensity I, which becomes a system of three DDEs when an additional optical feedback term is introduced [25]:

$$\begin{aligned}\dot{G}(t) &= \Gamma_G[A - G(t) - G(t)I(t)],\\ \dot{Q}(t) &= \Gamma_Q[B - Q(t) - aQ(t)I(t)],\\ \dot{I}(t) &= (G(t) - Q(t) - 1)I(t) + \eta I(t-\tau). \end{aligned} \quad (1)$$

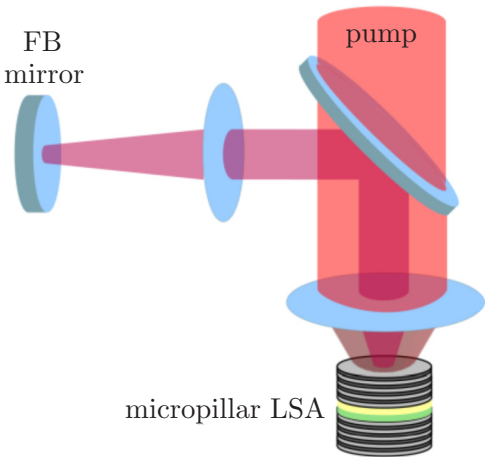

FIG. 1. Sketch of a semiconductor micropillar laser with an integrated saturable absorber section, pumped optically, and subject to delayed optical feedback from an external mirror [10].

Here, Γ_G and Γ_Q are the recombination rates of carriers in the gain and absorber sections, respectively, a is the saturation parameter, A is the pump level, and B is the linear absorption. Furthermore, η and τ are the feedback strength and feedback delay, respectively. All the time variables are rescaled with respect to the photon lifetime $\tau_{\rm ph}$ in the cavity [7]. Importantly, this model only describes the evolution of the intensity of the electric field. In particular, the phase of the electric field is not taken into account and the feedback is modeled as being incoherent: no phase relationship is considered between the electric field at instant t and that at instant $t-\tau$. Although this may appear to be a major limitation, the Yamada model with feedback has been shown to be valid for a microlaser with feedback like the one sketched in Fig. 1. In particular, it shows very good agreement with experimental observations, when the pulses are short compared to the delay time [10,26].

The DDE MLL model for mode-locked lasers, on the other hand, was originally derived from the standard traveling-wave equations for semiconductor lasers under the assumption of unidirectional propagation [17,27]. As such, it describes the mode-locked dynamics of a ring cavity semiconductor laser, as represented schematically in Fig. 2. In the case without feedback, it is a system of three DDEs already, which has been extended to include delayed optical feedback from one or more external cavities [28]. It is then written as a system of three

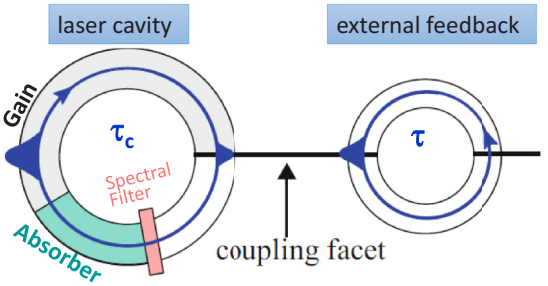

FIG. 2. Sketch of a ring-cavity semiconductor laser with an integrated saturable absorber (LSA) section, spectral filtering, and one external feedback (FB) cavity.

TABLE I. Parameter values used in numerical simulations of Eq. (1) and Eqs. (3)–(5), respectively, with physical units where appropriate.

Symbol	Value	Symbol	Value
Γ_G ($\widetilde{\gamma}_g$)	0.0125 (1 ns^{-1})	Γ_Q ($\widetilde{\gamma}_q$)	0.9375 (75 ns^{-1})
a	1.04	$\widetilde{\tau}_{\mathrm{ph}}$	12.5 ps
γ_g ($\widetilde{\gamma}_g$)	0.00625 (1 ns^{-1})	γ_q ($\widetilde{\gamma}_q$)	0.4675 (75 ns^{-1})
r_s	78.0	τ_c ($\widetilde{\tau}_c$)	1 (6.25 ps)
κ	0.34	γ ($\widetilde{\gamma}$)	1 (0.16 ps^{-1})

DDEs for the complex electric field $E(t)$ at the outcoupling facet, as well as the gain $\mathcal{G}$ and the absorption $\mathcal{Q}$ integrated over one internal round-trip:

$$\dot{E}(t) = -\gamma E(t) + \gamma R(t-\tau_c)e^{-i\Delta\Omega\tau_c}E(t-\tau_c) + K\,e^{-iC}\gamma R(t-\tau_c-\tau)e^{-i\Delta\Omega(\tau_c+\tau)}E(t-\tau_c-\tau), \tag{2}$$

$$\dot{\mathcal{G}}(t) = J_g - \gamma_g\mathcal{G}(t) - e^{-\mathcal{Q}(t)}(e^{\mathcal{G}(t)}-1)|E(t)|^2, \tag{3}$$

$$\dot{\mathcal{Q}}(t) = J_q - \gamma_q\mathcal{Q}(t) - r_s e^{-\mathcal{Q}(t)}(e^{\mathcal{Q}(t)}-1)|E(t)|^2, \tag{4}$$

with

$$R(t) = \sqrt{\kappa}e^{\frac{1}{2}((1-i\alpha_g)\mathcal{G}(t)-(1-i\alpha_q)\mathcal{Q}(t))}.$$

Here, α_g and α_q are the linewidth enhancement factors in the gain and absorber sections, respectively, and γ and $\Delta\Omega$ are the width and the center frequency of the spectral filter element. Further, τ_c is the internal round-trip time, and κ describes the outcoupling losses such that a fraction $\sqrt{\kappa}E(t)$ of the light remains in the cavity. The delayed optical feedback is described by the feedback strength K, the delay τ, and the feedback phase shift C. Moreover, J_g and J_q, on the one hand, and γ_g and γ_q, on the other hand, are the pump parameters and the recombination rates of carriers in the gain and the absorber section, respectively. Finally, the saturation energy ratio is represented by the parameter r_s. For numerical purposes, the time variables and parameters, as well as the rates, are rescaled (either multiplied or divided) by the round-trip time $\widetilde{\tau}_c$ [29]. In particular, this means that $\tau_c = 1$ in Eqs. (2)–(4); nevertheless, we keep τ_c explicitly in this and the following formulas for clarity. It is noteworthy that in systems (1) and (2)–(4), each variable evolves on its own time scale, which is modeled by the parameters Γ_G and Γ_Q in the Yamada model and γ_g and γ_q in the DDE MLL model; the different parameters and their chosen values are listed in Table I. Equations (1) and (2)–(4) are slow-fast dynamical systems with three different time scales. The dynamics of such systems is of theoretical and practical interest, beyond the particular models considered here; see, for example, [30].

A. From the DDE MLL model to the Yamada model

Although both models rely on different assumptions, they are derived from the same physical principles. We now show how the Yamada model, (1), can be related directly to the DDE MLL model, (2)–(4). Assuming that the frequency maximum of the spectral filter coincides with the gain maximum, $\Delta\Omega$ is 0. Assuming further, as in [21] and [28], $\alpha_g = \alpha_q = 0$ and a vanishing phase shift $C = 0$, the electric field becomes real. Moreover, the feedback term in system (2)–(4) is included such that the light enters from the back facet and has to go through the ring cavity before one round-trip is complete (see Fig. 2). In principle, this leads to a gain- and loss-dependent feedback strength, which can be assumed to be constant for small gain $\mathcal{G}$ and absorption $\mathcal{Q}$, in particular, in small devices. One can then write

$$\dot{E}(t) = -\gamma E(t) + \gamma\sqrt{\kappa}e^{\frac{1}{2}(\mathcal{G}(t-\tau_c)-\mathcal{Q}(t-\tau_c))}E(t-\tau_c) + K\gamma\sqrt{\kappa}E(t-\tau_c-\tau). \tag{5}$$

In Eq. (5), the derivative includes all temporal changes during one internal round-trip within the device. When the electric field envelope evolves slowly in time and thus does not change much during one internal round-trip, one can neglect the left-hand-side term $\gamma^{-1}\dot{E}(t)$ in Eq. (5). Under this assumption we can define a new derivative describing only the slow changes between round-trips by [31,32]

$$E(t-\tau_c) \approx E(t) - \tau_c\frac{dE}{dt}. \tag{6}$$

The assumption is well satisfied for the rather long Q-switched pulses and we arrive at the equation

$$\frac{dE(t)}{dt} = \frac{1}{\tau_c}\{-E(t) + e^{\frac{1}{2}[ln(\kappa)+\mathcal{G}(t)-\mathcal{Q}(t)]}E(t) + K\sqrt{\kappa}E(t-\tau)\},$$

where $\mathcal{G}$ and $\mathcal{Q}$ are now evaluated at time t rather than time $t-\tau_c$. Note, further, that the effect of outcoupling losses is still included and described by κ. Linearizing the exponential term with the argument of small gain $\mathcal{G}$ and absorption $\mathcal{Q}$ and redefining $\widetilde{G} = \mathcal{G}/\tau_c$ and $\widetilde{Q} = \mathcal{Q}/\tau_c$, as well as introducing the intensity $\mathcal{I} = |E|^2$, one eventually obtains

$$\begin{aligned}
\dot{\widetilde{G}} &= \frac{J_g}{\tau_c} - \gamma_g\widetilde{G}(t) - \widetilde{G}(t)\mathcal{I}(t),\\
\dot{\widetilde{Q}} &= \frac{J_q}{\tau_c} - \gamma_q\widetilde{Q}(t) - r_s\widetilde{Q}(t)\mathcal{I}(t),\\
\dot{\mathcal{I}} &= \left[\widetilde{G}(t) - \widetilde{Q}(t) + \frac{ln(\kappa)}{\tau_c}\right]\mathcal{I}(t) + \frac{2K\sqrt{\kappa}}{\tau_c}E(t-\tau)E(t).
\end{aligned} \tag{7}$$

It has been shown theoretically that, in the limit of pulsing dynamics, one can consider, again in first approximation, that $KE(t-\tau)E(t) \approx \widetilde{K}\mathcal{I}(t-\tau)$. In particular, a bifurcation analysis shows that both terms lead to identical qualitative dynamics [26]. By defining the dimensionless variables and parameters as in [9], one eventually obtains the Yamada model with feedback, (1).

A serious difficulty for the comparison of both models is the matching of parameters. We consider identical values for the physical parameters $\widetilde{\gamma}_g = 1$ ns^{-1}, $\widetilde{\gamma}_q = 75$ ns^{-1}, and $r_s = 78$. Here, a tilde above a symbol indicates the nonrescaled value; these are chosen to match the parameter values commonly considered in the literature for the DDE MLL model, (2)–(4) [29]. It is noteworthy that the values of $\widetilde{\gamma}_g$ and $\widetilde{\gamma}_q$, which describe the time scales on which the gain and absorption

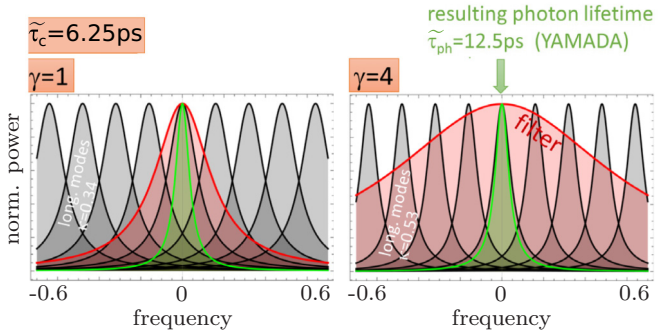

FIG. 3. Schematic of the relative contributions of the filter width γ and the round-trip losses (modeled through the ratio κ) to the photon lifetime $\widetilde{\tau}_{ph}$ in the DDE MLL model, (3)–(5), for a fixed value of the round-trip time $\widetilde{\tau}_c$. For a small filter width (left), $\widetilde{\tau}_{ph}$ depends on both the round-trip losses and the bandwidth of the spectral filter element, while for a large filter width (right), $\widetilde{\tau}_{ph}$ is constrained only by the round-trip losses.

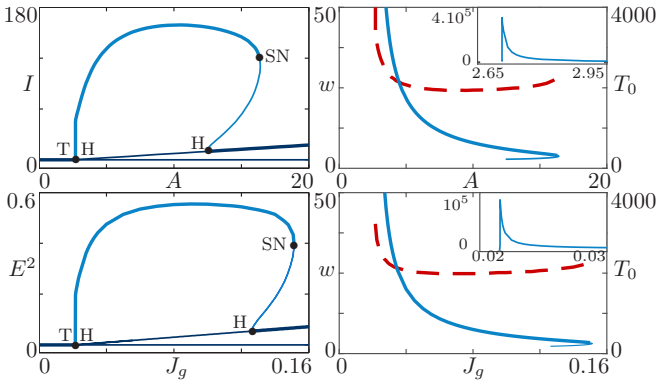

FIG. 4. Bifurcation diagrams of model (1) (top) and model (3)–(5) with $\gamma = 1$ (bottom), with respect to the pump parameter. Left: Amplitude of the intensity variable, where the equilibrium and periodic solutions are in dark and light blue, respectively. Solutions are stable along thick parts of the curves. T and H, transcritical and Hopf bifurcations, respectively; SN, saddle-node bifurcations of periodic orbits. Right: Period T_0 in ps (solid blue line) and pulse width w in ps (dashed red line) along the branch of periodic solutions. Inset: Evolution of T_0 near the leftmost Hopf bifurcation.

variables evolve, differ considerably from the values usually considered for the Yamada model [7,9,10]. In what follows, we consider Eqs. (3)–(5), and we take into account a single mode by setting $\gamma = 1$ (corresponding to a physical filter width of $\widetilde{\gamma} = \gamma/\widetilde{\tau}_c$), so that mode-locking cannot occur. Importantly, a change in the filter width γ induces an effective change in the total photon lifetime τ_{ph} in the cavity. The photon lifetime inherent in the DDE MLL model is defined via exponential decay of the electric field; using $E(t) \sim \exp[-\frac{t}{2\tau_{ph}}]$ in Eq. (5) without gain, absorption, and feedback, which yields the transcendental equation,

$$\tau_c = 2\tau_{ph}\gamma\left(1 - \sqrt{\kappa}\exp\left[\frac{\tau_c}{2\tau_{ph}}\right]\right). \tag{8}$$

In the limit of large γ this gives $\tau_{ph} = -\tau_c/\ln(\kappa)$. In physical units this gives $\widetilde{\tau}_{ph}^{\gamma=100} = 5.9$ ps for the values $\kappa = 0.34$ and $\widetilde{\tau}_c = 6.25$ ps considered hereafter; see Fig. 3. For our smaller filter width $\gamma = 1$, this gives $\widetilde{\tau}_{ph}^{\gamma=1;\kappa=0.34} = 12.5$ ps, which is the value considered hereafter to rescale the parameters of the Yamada model, (1). Overall, keeping τ_{ph} constant when γ is varied implies that one needs to adapt the round-trip losses, which are modeled through the factor κ and relate to the Q factor of the cavity modes. Relationships between the pump and the linear absorption parameters of both models can be derived analytically and are given in the Appendix.

III. DYNAMICS WITHOUT EXTERNAL FEEDBACK

The dynamics of the Yamada model and the DDE MLL model have been studied extensively in the case without external feedback (given by $K = 0$ and $\eta = 0$) [9,17,29]. Compared to the literature, we consider here a different regime of operation: namely, a Q-switched pulsing regime with $\gamma = 1$ for the DDE MLL model and different time scales Γ_G and Γ_Q associated with the gain G and absorption Q for the Yamada model. We focus on the existence of Q-switched pulsing regimes and on the dependence of the pulse width w and pulse period T_0 on both the pump and the linear absorption parameters.

In actual experiments, the pump is the main control parameter and it is associated with the amount of energy provided to the gain section of the lasers. Figure 4 shows one-parameter bifurcation diagrams of both models for fixed absorption levels ($J_q = 1.1$ and $B = 1.7$), when the pump level is considered as a bifurcation parameter. This shows that the qualitative dynamics is identical in the two models. In particular, the same bifurcation scenario is observed when the pump is increased from 0: for low pump, the laser is on a nonlasing equilibrium, which becomes unstable at the laser thresholds through a transcritical bifurcation T. The laser subsequently settles on another stable equilibrium with nonzero intensity, the so-called continuous-wave solution, which corresponds to the emission of a constant beam of light. These equilibria almost immediately become unstable through a supercritical Hopf bifurcation H. At this point, a stable periodic orbit emerges, whose amplitude and period grow rapidly when the pump is increased: it then corresponds to the emission of short pulses of light, between which the light intensity is practically 0. At $J_g = 0.13$ and $A = 16.8$, this stable periodic orbit collides, in a saddle-node bifurcation, with a periodic orbit of the saddle type which previously emerged from a subcritical Hopf bifurcation of the continuous-wave equilibrium. At this point, the laser settles back on the lasing equilibrium, which is the only stable solution. One can note that the sudden increase in the amplitude of the periodic solution around $J_g = 0.02$ (for the DDE MLL model) and $A = 1.7$ (for the Yamada model), combined with the large but finite value of the period T_0, suggests a canard explosion [33]. This phenomenon is typical of slow-fast dynamical systems where variables evolve on different time scales [34]. Its investigation is beyond the scope of this article and will be discussed elsewhere.

We now investigate how the bifurcation scenario evolves when the linear absorption parameter is changed. Figure 5 represents the two-parameter bifurcation diagrams of both models when the pump (J_g and A) and the linear absorption

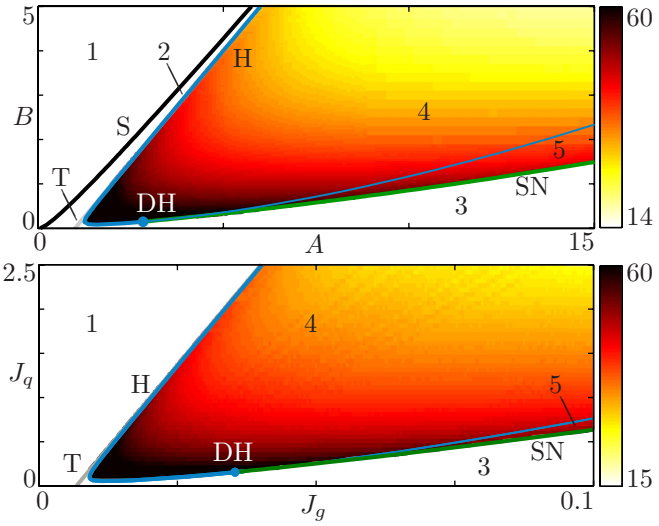

FIG. 5. Bifurcation diagrams of models (1) (top) and (3)–(5) (bottom) in the (A, B) plane and (J_g, J_q) plane, respectively. Curves: S, saddle-node bifurcation; T, transcritical bifurcation; H, Hopf bifurcation; SN, saddle-node bifurcation of periodic orbits emerging from a degenerate Hopf bifurcation point, DH. Along thick parts of curve H the Hopf bifurcation is supercritical. In regions 4 and 5, the pulse width w (in ps) is represented by color.

(J_q and B) are considered as bifurcation parameters. In the parameter plane, each curve corresponds to the locus of a specific codimension-one bifurcation. More specifically, one finds

(i) a curve (S) of saddle-node bifurcation, where a stable and a saddle equilibrium bifurcate;

(ii) a curve (T) of transcritical bifurcation, corresponding to the lasing threshold, where the zero-intensity equilibrium change stability;

(iii) a curve (H) of Hopf bifurcation, where the lasing equilibrium changes stability and a periodic solution emerges, which is locally stable (unstable) when the Hopf bifurcation is supercritical (subcritical);

(iv) a degenerate Hopf point (DH) where the Hopf bifurcation changes criticality; and

(v) a curve (SN) of saddle-node bifurcation of periodic orbits emerging from the point DH, where one stable and one saddle-type periodic orbit collide and disappear.

The different bifurcation curves divide the parameter plane into regions where the dynamics is qualitatively different. In region 1, the only solution is a stable zero-intensity (i.e., nonlasing) equilibrium. In region 2, the stable nonlasing equilibrium coexists with one additional stable (continuous-wave) equilibrium and one saddle-type equilibrium. Entering region 3 from region 2, the nonlasing equilibrium becomes unstable so that the continuous-wave regime is the only stable solution. In region 4, all the equilibria are unstable, and the only stable solution is a periodic solution. In region 5, all the solutions of region 4 remain and coexist with an additional saddle-type periodic orbit. In regions 4 and 5, the width of the stable pulsing periodic solution estimated at half the maximum of the intensity [$|E|^2$ for (3)–(5) and I for (1)] is represented in Fig. 5 by the color map. The values differ slightly between the

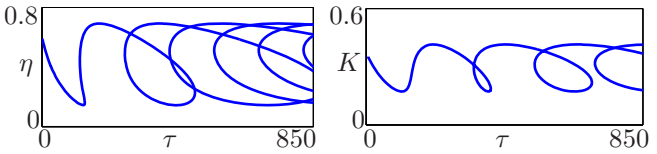

FIG. 6. Hopf bifurcation curves of models (1) (left) and (3)–(5) (right) in the plane of feedback delay τ (in ps) and feedback strength η and K. The parameter values $(A, B) = (9.34, 3.36)$ and $(J_g, J_q) = (0.063, 1.1)$ agree according to the conversion given in Appendix but yield different pulse profiles without feedback.

two models; however, the orders of magnitude are similar and the same trend is observed with respect to both continuation parameters. In particular, the width increases dramatically for small values of the absorption parameter. For a given value of this parameter, the pulse width is almost constant over a large range of the pump parameter and increases dramatically for small values of the pump. This trend was already highlighted in Fig. 4 for a single value of the linear absorption parameter.

Importantly, the range of parameters represented in Fig. 5 corresponds to identical nondimensionless values for both models (see the conversion given in the Appendix). With no feedback, both models thus show very good qualitative and quantitative agreement for identical values of the physical parameters. In particular, the same stable regimes (continuous wave or Q-switched) are observed, and for the Q-switched regime the pulse width and pulse repetition rates have similar values.

IV. MATCHING THE MODELS IN THE PRESENCE OF FEEDBACK

We consider now the effect of delayed feedback on the dynamics when the solitary laser is in the Q-switched pulsing regime. We focus on Hopf bifurcations, which are of particular interest since they correspond to the emergence of (pulsing) periodic solutions. An important motivation is to understand the conditions under which the DDE MLL model, (3)–(5), can be approximated accurately by the Yamada model, (1), which may considerably simplify numerical and theoretical investigation.

We consider fixed values $J_g = 0.063$ and $J_q = 1.1$ for (3)–(5), which correspond to $A = 9.34$ and $B = 3.36$ in (1); see the analytical expressions in the Appendix. Figure 6 represents the Hopf bifurcation curves of both models in the plane of feedback delay τ and feedback strength [η for (1) and K for (3)–(5)]. Some common features are observed: in both models, a single curve H is found, which displays the generic repeating property of delay systems [35], and self-intersects in codimension-two Hopf-Hopf bifurcation points [36]. However, more self-intersections of H are observed for model (1); in particular, one observes *secondary* self-intersections, where the loops generated by the *primary* self-intersections overlap. Generally, branches of torus bifurcation, associated with the emergence of quasiperiodic oscillations and the change in stability of periodic solutions, emanate from Hopf-Hopf bifurcation points [36]. As such, more self-intersections of the Hopf bifurcation curve strongly suggest that the overall bifurcation diagram is more complex.

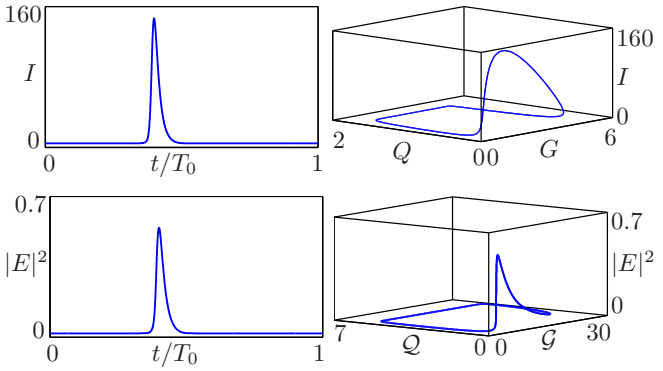

FIG. 7. Intensity time series (left) and phase portrait in the physical space (right) of the pulsing solution of model (1) (top) and (3)–(5) (bottom) without feedback, for $(A, B) = (7.9, 1.7)$ and $(J_g, J_q) = (0.063, 1.1)$, chosen to yield a pulse width of $w \approx 24.5$ ps and a pulse period of $T_0 \approx 35 \times w$ in both cases.

Figure 6 demonstrates that considering identical values of the parameters does not capture the essence of the feedback-induced dynamics. We showed in Fig. 5 that the pulsing characteristics of both models without feedback match for a range of pump and absorption levels. As we show now, the key is to choose the parameters of (1) and (3)–(5) such that the pulse width and period of the Q-switched solutions are identical for the solitary lasers (i.e., without feedback). Figure 7 represents the pulsing solutions of (1) and (3)–(5), without feedback, for $(A, B) = (7.9, 1.7)$ and $(J_g, J_q) = (0.063, 1.1)$, respectively, chosen to yield similar laser outputs. In both models, the pulse width is close to 24.5 ps, and the pulse period T_0 is 35 times as large. Although the match is not perfect, Fig. 7 shows that in both models the pulse shape is strongly asymmetrical, and the dynamics mainly takes place in two planes close to $(G, Q, 0)$ and (G, Q_0, I) for (1) and to $(\mathcal{G}, \mathcal{Q}, 0)$ and $(\mathcal{G}, \mathcal{Q}_0, E)$ for (3)–(5), where Q_0 and $\mathcal{Q}_0$ are constants. This is related to the different time scales on which the variables evolve, represented by $\widetilde{\gamma}_g$ and $\widetilde{\gamma}_q$. The exact nature of the influence of these time scales on the lasers dynamics is beyond the scope of this paper; it will be discussed elsewhere.

For these matched values of (A, B) and (J_g, J_q), Fig. 8 shows the curves of Hopf bifurcations of (1) and (3)–(5) in the plane of feedback parameters. The two models now show very good agreement on the level of Hopf bifurcations: not only is a single curve H observed in both models, but also they self-intersect in a very similar manner. In particular, the primary self-intersections occur for very similar values of τ, and no secondary self-intersection is observed.

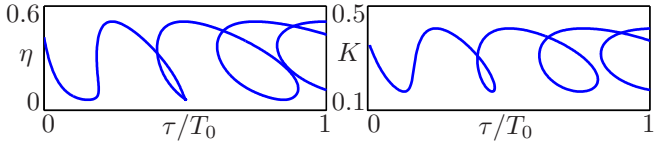

FIG. 8. Hopf bifurcation curves of (1) (left) and (3)–(5) (right) in the plane of feedback delay and feedback strength, for $(A, B) = (7.9, 1.7)$ and $(J_g, J_q) = (0.063, 1.1)$, respectively, chosen such that without feedback ($\eta = 0$ and $K = 0$), both systems are pulsing with pulse width $w = 24.5$ ps and pulse period $T_0 = 850$ ps.

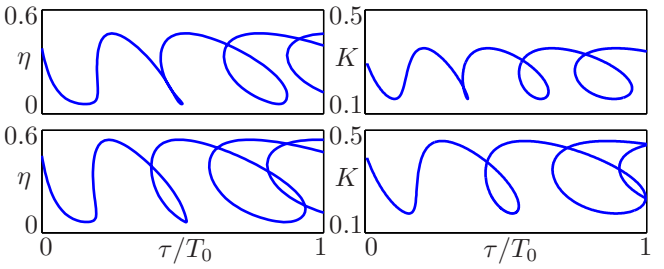

FIG. 9. Hopf bifurcation curves of (1) (left) and (3)–(5) (right) in the plane of feedback parameters. From top to bottom: $B = 1.9$ and $B = 1.5$ (left); and $J_q = 1.5$ and $J_q = 0.8$ (right). Values of A and J_g are chosen so that, without feedback, the pulse period–to–pulse width ratio is 35.

A. Influence of the pulse width and period

We now demonstrate that the good agreement of (1) and (3)–(5) on the level of H exists over a wide range of other parameters, provided that the pulse width and pulse period are identical in the solitary laser. The results in Fig. 8 were obtained for a pulse width $w = 24.5$ ps in the solitary laser. We now investigate the feedback-induced dynamics when $w = 22.5$ ps and $w = 26.5$ ps, which is achieved for $B = 1.9$ and $B = 1.5$ in (1) and $J_q = 1.5$ and $J_q = 0.8$ in (3)–(5), respectively. The values of the pump parameters A and J_g are chosen such that the period-to-width ratio remains, as before, close to 35. For these parameters, Fig. 9 presents the curves of Hopf bifurcation in the plane of feedback parameters. Although the exact values of τ at which H self-intersects do not match perfectly, the results are very similar in terms of the numbers of both primary and secondary self-intersections of H. Overall, Fig. 8 and 9 show that a wider pulse (corresponding to a lower absorption level; see Fig. 5) is associated with more self-intersections of H.

We now investigate the influence of the pulse period T_0 of the solitary laser on the feedback-induced dynamics. We consider the same three values of the pulse width w as in Figs. 8 and 9 (that is, the same values of the absorption parameters), but we now choose the pump level such that the period-to-width ratio is close to 50 in the solitary laser. Figure 10 represents the corresponding curves H of Hopf bifurcation in the plane of feedback parameters, again showing very good agreement between the models. As before, a wider pulse (that is, a lower absorption level) results in more self-intersections of H. Moreover, comparison of Fig. 10 with Figs. 8 and 9 shows that a higher period-to-width ratio in the solitary laser (i.e., a lower pump level; see Fig. 5) also results in more self-intersections of H.

We checked that these results are robust to a change of the round-trip time $\widetilde{\tau}_c$ in the DDE MLL model. Considering $\widetilde{\tau}_c = 3.125$ ps (i.e., half of the value considered here) and adjusting the ratio κ (associated with round-trip losses) such that the photon lifetime remains equal to 12.5 ps, the curve H in the plane of feedback parameters is practically unchanged from the one in Fig. 8, provided that the solitary laser features an identical pulse width and pulse period.

The very good agreement between the two models on the level of curve H strongly suggests that the feedback-induced dynamics in models (1) and (3)–(5) can be matched for a large

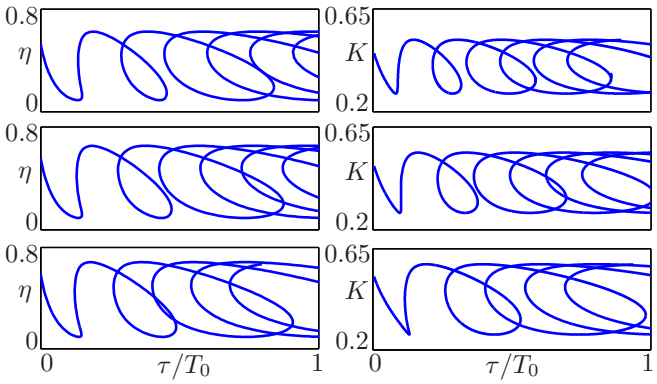

FIG. 10. Hopf bifurcation curves of (1) (left) and (3)–(5) (right) in the plane of feedback parameters. From top to bottom: $B = 1.9$, $B = 1.7$, and $B = 1.5$ (left); $J_q = 1.5$, $J_q = 1.1$, and $J_q = 0.8$ (right). Values of A and J_g are chosen so that, without feedback, the pulse period–to–pulse width ratio is 50.

range of parameters. The clear conclusion is that what matters is indeed maintaining the value of the pulse width and pulse period in the solitary laser.

B. Feedback-induced dynamics

The motivation for matching the Hopf bifurcation curves of both models was the fact that they organize the overall pulsing dynamics. We now investigate in more detail this feedback-induced dynamics for a particular set of laser parameters. Figure 11 represents the overall bifurcation diagrams of both models in the plane of feedback parameters, for the same pump and absorption levels as considered in Fig. 8. We

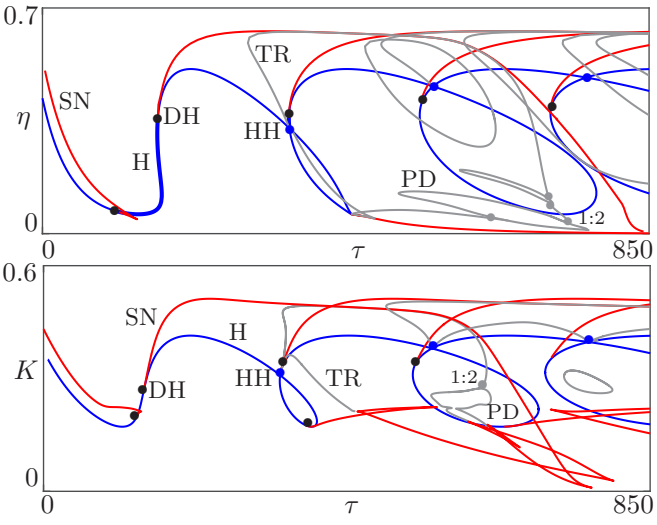

FIG. 11. Bifurcation diagram of (1) (top) and (3)–(5) (bottom) in the plane of feedback delay τ (in ps) and feedback strength, for $(A, B) = (7.9, 1.7)$ and $(J_g, J_q) = (0.063, 1.1)$, respectively. The solitary laser is in the Q-switched regime, with a pulse width of 24.5 ps and a pulse period 35 times as large. Curves: H, Hopf bifurcations; SN, saddle-node bifurcations of periodic orbits emerging from degenerate Hopf points, DH; TR, torus bifurcations emerging from Hopf-Hopf bifurcation points, HH; PD, period-doubling bifurcations.

now represent the criticality of the Hopf bifurcation: along thick parts of curve H, the Hopf bifurcation is supercritical, meaning that the emerging periodic solution is locally stable, while it is locally unstable when the Hopf bifurcation is subcritical [36]. The points DH at which the Hopf bifurcation changes criticality are degenerate Hopf bifurcation points, from which the SN curves emerge [36]. These curves form the locus of saddle-node bifurcations of periodic orbits, where one stable and one saddle-type periodic orbit collide and disappear. TR curves of torus bifurcation are also represented, which emerge from Hopf-Hopf bifurcation points where the Hopf bifurcation curve self-intersects. Torus bifurcations can lead to stable quasiperiodic dynamics; this is discussed in [21] for the DDE MLL model and in [26] for the Yamada model. Finally, one finds PD curves of period-doubling bifurcations, which emerge from 1:2 resonant points along the TR curve [36].

In Fig. 11, curve H changes criticality in a similar manner for (1) and (3)–(5), and the SN curves cross curve H for similar values of τ. In both models, these SN curves interact in pairs at cusp bifurcations points when the feedback strength becomes close to 0. Since Hopf bifurcations and saddle-node bifurcations correspond to the emergence and the disappearance of periodic solutions, respectively, these similarities strongly suggest that different periodic solutions exist and are stable for similar ranges of τ in both models. The torus bifurcation curves also show similar qualitative behavior in (1) and (3)–(5); in particular, one finds isolated closed TR curves, which do not connect to a point HH. The torus bifurcations are of practical interest beyond the possible emergence of quasiperiodicity: although most parts of the H curves correspond to subcritical Hopf bifurcations, meaning that the emerging periodic solution is unstable, several of these unstable periodic solutions stabilize via a torus bifurcation when the delay τ is increased. As a consequence, there is a high degree of multistability in different regions of the plane of feedback parameters, with the coexistence of several stable pulsing periodic solutions [21,26].

Although both models show an overall good qualitative agreement, differences are observed in the finer details of the dynamics. The DDE MLL model, (3)–(5), features multiple cusp points along the SN curves and 1:1 resonances where TR curves connect with SN curves. Nevertheless, overall the bifurcation diagrams of the DDE MLL model and the Yamada model show good qualitative and quantitative agreement, considering that the modeling approaches are very different from each other.

V. INFLUENCE OF THE NUMBER OF MODES

When a single cavity mode is considered ($\gamma = 1$), we have shown that the dynamics of the DDE MLL is represented accurately by the simpler Yamada model. We now investigate the influence of a larger, but still small, number of cavity modes on the dynamics of the DDE MLL model without feedback. Our focus is on the properties of the Q-switched pulsing solution, which are the key for matching both models. We consider $\gamma = 8$ and set $\kappa = 0.58$ such that the photon lifetime remains $\widetilde{\tau}_{\rm ph} = 12.5$ ps (see Fig. 3). Figure 12(a) shows the bifurcation diagram of model (3)–(5) in the (J_g, J_q) plane, when no feedback is considered ($K = 0$). As for the

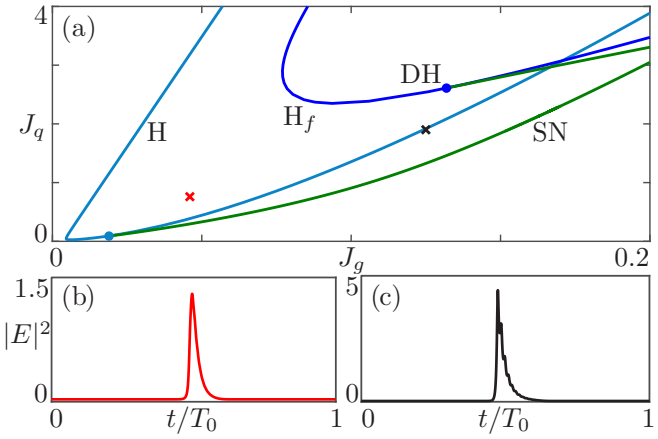

FIG. 12. (a) Bifurcation diagram of (3)–(5) in the (J_g, J_q) plane, for $\gamma = 8$ and $\kappa = 0.58$. Displayed are two curves, H and H_f, of Hopf bifurcations, associated with Q-switching and fundamental mode-locking, respectively, and two curves, SN, of saddle-node bifurcations of periodic orbits, emerging from degenerate Hopf bifurcation points, DH. (b) Intensity profile of the Q-switched periodic solution for values of (J_g, J_q) indicated by the red and black x's, respectively, in (a).

single-mode case in Fig. 5, one finds a curve H of Hopf bifurcation where the Q-switched pulsing periodic solution is born, and a curve (SN) of saddle-node bifurcation of periodic orbits emanating from a degenerate Hopf bifurcation point DH. Compared to Fig. 5, an additional curve H_f is found, where the fundamental mode-locked periodic solution is born: this is a pulsing solution with a period close to the round-trip time τ_c of the device [29].

Figure 12 also shows the intensity profile of the Q-switched solution for two different sets of (J_g, J_q). Compared to the case $\gamma = 1$, the pulse shape is not affected for low values of J_q. On the other hand, it deforms when one approaches curve H_f: one observes a *multipulse* profile with several intensity peaks within one period. This strongly suggests that the feedback-induced dynamics of the DDE MLL model can still be represented accurately by the Yamada model for small values of J_q, but no longer for larger absorption levels, close to the second H_f curve on the (J_g, J_q) plane. When the number of modes γ is increased further, several additional curves of Hopf bifurcation, associated with mode-locked regimes of higher order (the so-called harmonic mode-locked regimes), move toward smaller values of J_q on the (J_g, J_q) plane. As a result, from about $\gamma = 10$, the Yamada model cannot be considered a valid representation of the DDE MLL model, neither for the solitary laser nor for the system with feedback.

We remark that decreasing the filter width γ below 1 in the DDE MLL model also induces a change in the pulse shape of the Q-switched solution, which then differs significantly from the one observed in the Yamada model. In that case, the feedback-induced dynamics is similar to the case $\gamma = 1$ when the values of J_g and J_q are chosen such that the area under the pulse (associated with the pulse energy) is kept constant, although this corresponds to a different pulse width. In this case, the dynamics of (3)–(5) in the plane of feedback parameters can still be represented accurately by (1).

VI. CONCLUSIONS

The effect of optical self-feedback on the dynamics of self-pulsing semiconductor lasers with gain and absorber sections was investigated. We compared two modeling approaches, the well-known Yamada model and the ring-cavity DDE MLL model, and characterized their bifurcation structure. We focused on the single-mode limit and on the Q-switching dynamics, even though the DDE MLL model is designed to describe the multimode effects of mode-locking.

Our results showed very good qualitative agreement between both modeling approaches over wide parameter regions. The bifurcation structures in the plane of feedback parameters show good qualitative and quantitative agreement as long as the pulse width and pulse period of the Q-switched solution are equal in both models without feedback. This is robust with respect to changes in the parameters, suggesting that the physical principles ruling the feedback-induced dynamics are caught by the properties of the Q-switched pulsing solution. The fact that the dynamics of the DDE MLL model is represented accurately by the simpler Yamada model in the single-mode limit is of practical interest, since this might simplify considerably numerical and theoretical investigations of self-pulsing lasers subject to delayed feedback.

Interestingly, these results are robust to a moderate increase in the number of modes in the DDE MLL. However, when the number of modes is too large, additional instabilities, in particular, mode-locked solutions, emerge. The region of stable Q-switched emission thus shrinks, and more complex pulse shapes of the Q-switched emission are observed in the vicinity of the new instabilities.

ACKNOWLEDGMENTS

We thank Dr. Benjamin Lingnau for fruitful discussions. This work was supported in part by the German Research Foundation (CRC 787). K.L. was supported by a Feodor Lynen Research Fellowship of the Alexander von Humboldt Foundation and thanks the University of Auckland for their hospitality and support.

APPENDIX: RELATIONSHIP BETWEEN THE PARAMETERS OF THE DDE MLL AND THE YAMADA MODELS

Starting from Eq. (7), which followed from the DDE MLL model in the limit of small changes during one round-trip, one can derive equations for the gain G and the absorption Q, written in the same form as the Yamada model, (1). As the first step, we rescale time to change from scaling with the round-trip time $\widetilde{\tau}_c$ to scaling with the photon lifetime $\widetilde{\tau}_{\rm ph}$ as in the Yamada model; recalling that $\tau_c = 1$, one obtains

$$\begin{aligned}
\dot{\widetilde{G}} &= \frac{\widetilde{\tau}_{\rm ph}}{\widetilde{\tau}_c} J_g - \Gamma_G \widetilde{G}(t) - \widetilde{G}(t)\mathcal{I}(t)\frac{\widetilde{\tau}_{\rm ph}}{\widetilde{\tau}_c}, \\
\dot{\widetilde{Q}} &= \frac{\widetilde{\tau}_{\rm ph}}{\widetilde{\tau}_c} J_q - \Gamma_Q \widetilde{Q}(t) - r_s \widetilde{Q}(t)\mathcal{I}(t)\frac{\widetilde{\tau}_{\rm ph}}{\widetilde{\tau}_c}, \\
\dot{\mathcal{I}} &= \frac{\widetilde{\tau}_{\rm ph}}{\widetilde{\tau}_c}\big[\widetilde{G}(t) - \widetilde{Q}(t) + \ln(\kappa)\big]\mathcal{I}(t) + \frac{2\widetilde{K}\sqrt{\kappa}\,\widetilde{\tau}_{\rm ph}}{\widetilde{\tau}_c}\mathcal{I}(t-\tau),
\end{aligned} \tag{A1}$$

where the decay rates $\Gamma_G = \gamma_g \widetilde{\tau}_{\rm ph}/\widetilde{\tau}_c$ and $\Gamma_Q = \gamma_q \widetilde{\tau}_{\rm ph}/\widetilde{\tau}_c$ and time are now scaled as in the Yamada equations. Factorizing out Γ_G and Γ_Q, and defining $I(t) = \widetilde{\tau}_{\rm ph}\mathcal{I}(t)/(\widetilde{\tau}_c\Gamma_G)$ as in [9] and $\eta = 2\widetilde{K}\sqrt{\kappa}\widetilde{\tau}_{\rm ph}/\widetilde{\tau}_c$, one obtains

$$\dot{\widetilde{G}} = \Gamma_G\left(\frac{J_g\widetilde{\tau}_{\rm ph}}{\widetilde{\tau}_c\Gamma_G} - \widetilde{G}(t) - \widetilde{G}(t)I(t)\right),$$

$$\dot{\widetilde{Q}} = \Gamma_Q\left(\frac{J_q\widetilde{\tau}_{\rm ph}}{\widetilde{\tau}_c\Gamma_Q} - \widetilde{Q}(t) - r_s\frac{\Gamma_G}{\Gamma_Q}\widetilde{Q}(t)I(t)\right),$$

$$\dot{I} = \frac{\widetilde{\tau}_{\rm ph} ln(\kappa)}{\widetilde{\tau}_c}\left[\frac{\widetilde{G}(t)}{\ln(\kappa)} - \frac{\widetilde{Q}(t)}{\ln(\kappa)} + 1\right]I(t) + \eta I(t-\tau). \quad \text{(A2)}$$

Redefining gain and absorption by $G = \widetilde{G}/\ln(\kappa)$ and $Q = \widetilde{Q}/\ln(\kappa)$, respectively, we arrive at

$$\dot{G} = \Gamma_G\left(\frac{J_g\widetilde{\tau}_{\rm ph}}{\widetilde{\tau}_c\ln(\kappa)\Gamma_G} - G(t) - G(t)I(t)\right),$$

$$\dot{Q} = \Gamma_Q\left(\frac{J_q\widetilde{\tau}_{\rm ph}}{\widetilde{\tau}_c\ln(\kappa)\Gamma_Q} - Q(t) - aQ(t)I(t)\right),$$

$$\dot{I} = \frac{\widetilde{\tau}_{\rm ph}\ln(\kappa)}{\widetilde{\tau}_c}[G(t) - Q(t) + 1]I(t) + \eta I(t). \quad \text{(A3)}$$

Finally, defining

$$A = \frac{J_g}{\gamma_g\ln(\kappa)} = \frac{J_g\widetilde{\tau}_{\rm ph}}{\widetilde{\tau}_c\Gamma_G\ln(\kappa)}, \quad B = \frac{J_q\widetilde{\tau}_{\rm ph}}{\widetilde{\tau}_c\Gamma_Q\ln(\kappa)} = \frac{J_q}{\gamma_q\ln(\kappa)},$$

$$a = r_s\frac{\gamma_g}{\gamma_q} = r_s\frac{\Gamma_G}{\Gamma_Q}$$

gives the Yamada model in the form of Eq. (1) and, thus, a conversion between the pump parameters in both models. However, since the photon lifetime resulting from the pure round-trip losses in the DDE MLL model [$\widetilde{\tau}_{\rm ph} \sim -\widetilde{\tau}_c/\ln(\kappa) = 5.8$ ps] and the one including the filter-induced losses [$\widetilde{\tau}_{\rm ph}^{\gamma=1;\kappa=0.34} = 12.5$ ps as given by Eq. (8)] differ, the factor $\widetilde{\tau}_{\rm ph}\ln(\kappa)/\widetilde{\tau}_c$ in the third equation can deviate from 1. In our case of a small filter width $\gamma = 1$ this factor is 2.158. This may be a reason why the dynamics observed after direct conversion of the pump parameters does not match perfectly between the Yamada and the DDE MLL model.

[1] J. Ohtsubo and P. Davis, Chaotic optical communication, in *Unlocking Dynamical Diversity: Optical Feedback Effects on Semiconductor Lasers*, edited by D. M. Kane and K. A. Shore (Wiley, New York, 2005).

[2] P. Grelu and N. Akhmediev, Dissipative solitons for mode-locked lasers, Nat. Photon. **6**, 84 (2012).

[3] M. Marconi, J. Javaloyes, S. Balle, and M. Giudici, How Lasing Localized Structures Evolve Out of Passive Mode Locking, Phys. Rev. Lett. **112**, 223901 (2014).

[4] T. Elsass, K. Gauthron, G. Beaudoin, I. Sagnes, R. Kuszelewicz, and S. Barbay, Control of cavity solitons and dynamical states in a monolithic vertical cavity laser with saturable absorber, Eur. Phys. J. D **59**, 91 (2010).

[5] A. G Vladimirov, U. Bandelow, G. Fiol, D. Arsenijević, M. Kleinert, D. Bimberg, A. Pimenov, and D. Rachinskii, Dynamical regimes in a monolithic passively mode-locked quantum dot laser, JOSA B **27**, 2102 (2010).

[6] T. Erneux, Q-switching bifurcation in a laser with a saturable absorber, J. Opt. Soc. Am. B **5**, 1063 (1988).

[7] S. Barbay, R. Kuszelewicz, and A. M. Yacomotti, Excitability in a semiconductor laser with saturable absorber, Opt. Lett. **36**, 4476 (2011).

[8] M. Yamada, A theoretical analysis of self-sustained pulsation phenomena in narrow-stripe semiconductor lasers, IEEE J. Quantum Electron. **29**, 1330 (1993).

[9] J. L. A. Dubbeldam and B. Krauskopf, Self-pulsations of lasers with saturable absorber: Dynamics and bifurcations, Opt. Commun. **159**, 325 (1999).

[10] S. Terrien, B. Krauskopf, N. G. R. Broderick, L. Andréoli, F. Selmi, R. Braive, G. Beaudoin, I. Sagnes, and S. Barbay, Asymmetric noise sensitivity of pulse trains in an excitable microlaser with delayed optical feedback, Phys. Rev. A **96**, 043863 (2017).

[11] P. W. Smith, Mode-locking of lasers, Proc. IEEE **58**, 1342 (1970).

[12] D. M. Kane and K. A. Shore (eds.), *Unlocking Dynamical Diversity: Optical Feedback Effects on Semiconductor Lasers* (John Wiley & Sons, New York, 2005).

[13] K. Lüdge (ed.), *Nonlinear Laser Dynamics: From Quantum Dots to Cryptography* (John Wiley & Sons, New York, 2012).

[14] J. Mulet and J Mork, Analysis of timing jitter in external-cavity mode-locked semiconductor lasers, IEEE J. Quantum Electron. **42**, 249 (2006).

[15] J. Javaloyes and S. Balle, Mode-locking in semiconductor fabry-perot lasers, IEEE J. Quantum Electron. **46**, 1023 (2010).

[16] A. G. Vladimirov, D. Turaev, and G. Kozyreff, Delay differential equations for mode-locked semiconductor lasers, Opt. Lett. **29**, 1221 (2004).

[17] A. G. Vladimirov and D. Turaev, Model for passive mode locking in semiconductor lasers, Phys. Rev. A **72**, 033808 (2005).

[18] K. Engelborghs, T. Luzyanina, and G. Samaey, *DDE-BIFTOOL v. 2.00: A Matlab Package for Bifurcation Analysis of Delay Differential Equations*, Technical report (Department of Computer Science, KU Leuven, Leuven, Belgium, 2001).

[19] K. Engelborghs, T. Luzyanina, and D. Roose, Numerical bifurcation analysis of delay differential equations using DDE-BIFTOOL, ACM Trans. Math. Softw. (TOMS) **28**, 1 (2002).

[20] J. Sieber, K. Engelborghs, T. Luzyanina, G. Samaey, and D. Roose, DDE-BIFTOOL v. 3.1 manual—Bifurcation analysis of delay differential equations, Technical report; arXiv:1406.7144 (2015).

[21] L. Jaurigue, B. Krauskopf, and K. Lüdge, Multipulse dynamics of a passively mode-locked semiconductor laser with delayed optical feedback, Chaos Interdisc. J. Nonlin. Sci. **27**, 114301 (2017).

[22] M. Georgiou and T. Erneux, Pulsating laser oscillations depend on extremely-small-amplitude noise, Phys. Rev. A **45**, 6636 (1992).

[23] G. H. M. van Tartwijk and M. San Miguel, Optical feedback on self-pulsating semiconductor lasers, IEEE J. Quantum Electron. **32**, 1191 (1996).

[24] L. Jaurigue, A. Pimenov, D. Rachinskii, E. Schöll, K. Lüdge, and A. G. Vladimirov, Timing jitter of passively-mode-locked semiconductor lasers subject to optical feedback: A semi-analytic approach, Phys. Rev. A **92**, 053807 (2015).

[25] B. Krauskopf and J. J. Walker, in *Bifurcation Study of a Semiconductor Laser with Saturable Absorber and Delayed Optical Feedback* (Wiley-VCH Verlag, Weinheim, 2012), pp. 161–181.

[26] S. Terrien, B. Krauskopf, and N. G. R. Broderick, Bifurcation analysis of the Yamada model for a pulsing semiconductor laser with saturable absorber and delayed optical feedback, SIAM J. Appl. Dyn. Syst. **16**, 771 (2017).

[27] B. Tromborg, H. E. Lassen, and H. Olesen, Traveling wave analysis of semiconductor lasers: Modulation responses, mode stability and quantum mechanical treatment of noise spectra, IEEE J. Quantum Electron. **30**, 939 (1994).

[28] C. Otto, K. Lüdge, A. G. Vladimirov, M. Wolfrum, and E. Schöll, Delay-induced dynamics and jitter reduction of passively mode-locked semiconductor lasers subject to optical feedback, New J. Phys. **14**, 113033 (2012).

[29] L. Jaurigue, Dynamics and Stochastic Properties of Passively Mode-Locked Semiconductor Lasers Subject to Optical Feedback, Ph.D. thesis, Technische Universitat Berlin, 2016.

[30] M. Krupa, N. Popović, N. Kopell, and H. G. Rotstein, Mixed-mode oscillations in a three time-scale model for the dopaminergic neuron, Chaos Interdisc. J. Nonlin. Sci. **18**, 015106 (2008).

[31] R. Lang and K. Kobayashi, External optical feedback effects on semiconductor injection laser properties, IEEE J. Quantum Electron. **16**, 347 (1980).

[32] G. H. M. van Tartwijk and D. Lenstra, Semiconductor lasers with optical injection and feedback, Quantum Semiclass. Opt. **7**, 87 (1995).

[33] E. Benoît, *Dynamic Bifurcations: Proceedings of a Conference Held in Luminy*, France, March 5–10, 1990 (Springer, Berlin, 2006).

[34] M. Desroches, J. Guckenheimer, B. Krauskopf, C. Kuehn, H. M. Osinga, and M. Wechselberger, Mixed-mode oscillations with multiple time scales, SIAM Rev. **54**, 211 (2012).

[35] S. Yanchuk and P. Perlikowski, Delay and periodicity, Phys. Rev. E **79**, 046221 (2009).

[36] Y. A. Kuznetsov, *Elements of Applied Bifurcation Theory*, Vol. 112 (Springer Science, Berlin, 2013).